



# Evidence of Müller Glia Conversion Into Retina Ganglion Cells Using Neurogenin2

Roberta Pereira de Melo Guimarães<sup>1,2,3†</sup>, Bruna Soares Landeira<sup>1†</sup>,  
Diego Marques Coelho<sup>1,4</sup>, Daiane Cristina Ferreira Golbert<sup>1</sup>, Mariana S. Silveira<sup>2</sup>,  
Rafael Linden<sup>2</sup>, Ricardo A. de Melo Reis<sup>3</sup> and Marcos R. Costa<sup>1\*</sup>

<sup>1</sup> Brain Institute, Federal University of Rio Grande do Norte, Natal, Brazil, <sup>2</sup> Lab Neurogenesis, Institute of Biophysics Carlos Chagas Filho, Federal University of Rio de Janeiro, Rio de Janeiro, Brazil, <sup>3</sup> Lab Neurochemistry, Institute of Biophysics Carlos Chagas Filho, Federal University of Rio de Janeiro, Rio de Janeiro, Brazil, <sup>4</sup> Bioinformatics Multidisciplinary Environment, IMD, Federal University of Rio Grande do Norte, Rio de Janeiro, Brazil

## OPEN ACCESS

### Edited by:

Sandra Henriques Vaz,  
Instituto de Medicina Molecular (IMM),  
Portugal

### Reviewed by:

Antje Grosche,  
Ludwig-Maximilians-Universität  
München, Germany  
Xiao-Feng Zhao,  
University of Michigan, United States

### \*Correspondence:

Marcos R. Costa  
mrcosta@neuro.ufrn.br

†These authors have contributed  
equally to this work

**Received:** 24 August 2018

**Accepted:** 22 October 2018

**Published:** 12 November 2018

### Citation:

Guimarães RPD, Landeira BS,  
Marques-Coelho D, Golbert DCF,  
Silveira MS, Linden R, de Melo Reis  
RA and Costa MR (2018) Evidence of  
Müller Glia Conversion Into Retina  
Ganglion Cells Using Neurogenin2.  
*Front. Cell. Neurosci.* 12:410.  
doi: 10.3389/fncel.2018.00410

Degenerative retinopathies are the leading causes of irreversible visual impairment in the elderly, affecting hundreds of millions of patients. Müller glia cells (MGC), the main type of glia found in the vertebrate retina, can resume proliferation in the rodent adult injured retina but contribute weakly to tissue repair when compared to zebrafish retina. However, postnatal and adult mouse MGC can be genetically reprogrammed through the expression of the transcription factor (TF) Achaete-scute homolog 1 (ASCL1) into induced neurons (iNs), displaying key hallmarks of photoreceptors, bipolar and amacrine cells, which may contribute to regenerate the damaged retina. Here, we show that the TF neurogenin 2 (NEUROG2) is also sufficient to lineage-reprogram postnatal mouse MGC into iNs. The efficiency of MGC lineage conversion by NEUROG2 is similar to that observed after expression of ASCL1 and both TFs induce the generation of functionally active iNs. Treatment of MGC cultures with EGF and FGF2 prior to Neurog2 or Ascl1 expression enhances reprogramming efficiencies, what can be at least partially explained by an increase in the frequency of MGCs expressing sex determining region Y (SRY)-box 2 (SOX2). Transduction of either Neurog2 or Ascl1 led to the upregulation of key retina neuronal genes in MGC-derived iNs, but only NEUROG2 induced a consistent increase in the expression of putative retinal ganglion cell (RGC) genes. Moreover, *in vivo* electroporation of Neurog2 in late progenitors from the neonatal rat retina, which are transcriptionally similar to MGCs, also induced a shift in the generation of retinal cell subtypes, favoring neuronal differentiation at the expense of MGCs and resuming the generation of RGCs. Altogether, our data indicate that NEUROG2 induces lineage conversion of postnatal rodent MGCs into RGC-like iNs *in vitro* and resumes the generation of this neuronal type from late progenitors of the retina *in vivo*.

**Keywords:** retina, müller glia cells, induced neurons, lineage-reprogramming, neurogenin2, Ascl1, retina ganglion cells

## INTRODUCTION

The retina is a unique tissue with highly organized architecture, known to be one of the most energetically demanding systems in the nervous system (Wong-Riley, 2010). Due to oxidative stress, trauma, or genetic mutations, gradual and irreversible cell death affects specific neuronal types in the retina (Athanasίου et al., 2013). For instance, retinal ganglion cells (RGCs) and their axons degenerate in glaucoma, a neurodegenerative disease associated with increased intraocular pressure, eventually leading to blindness (Kimura et al., 2017). In the last 5 years almost 65 million people worldwide were diagnosed with glaucoma (Gill et al., 2016; Liang et al., 2017), which is the leading cause of visual impairment in developed countries (WHO). Still, despite the social and economic burden of such disease, therapeutic approaches are limited. Recent progress in cell-based therapy may, nonetheless, provide novel means to restore vision in glaucoma patients (Abu-Hassan et al., 2015; Chamling et al., 2016).

Cell lineage-reprogramming techniques, which allow the direct conversion of a non-neuronal cell into neurons, offer a powerful strategy to regenerate neuronal cells in the injured retina. In fact, expression of the bHLH neurogenic transcription factor (TF) Achaete-scute homolog 1 (ASCL1) *in vitro* induced the reprogramming of mouse Müller glia cells (MGC) into bipolar cells and, to a lesser extent, amacrine cells (Pollak et al., 2013). Following NMDA-mediated injury in postnatal mouse retina, ASCL1 expression reprogrammed MGCs into neurons expressing markers of bipolar cells, amacrine cells and photoreceptors (Ueki et al., 2015). Notably, when combined with the inhibitor of histone deacetylases trichostatin A, expression of ASCL1 elicited the conversion of some MGC into bipolar (~18%) and amacrine (~3%) cells in the injured adult retina (Jorstad et al., 2017). These findings demonstrate that regenerative effects of transgenic expression of ASCL1 in the adult mouse Müller glia are more limited as compared to the regenerative response observed in non-mammalian vertebrates (Wilken and Reh, 2016). Moreover, ASCL1 expression is not sufficient to reprogram MGCs into RGCs either *in vitro* or *in vivo* (Pollak et al., 2013; Ueki et al., 2015; Jorstad et al., 2017).

During development, expression of ASCL1 defines a subset of retinal progenitor cells (RPCs) that generate all neuronal types in the retina, except RGCs (Brzezinski et al., 2011). In contrast, expression of the bHLH TF Neurogenin 2 (NEUROG2) defines a separate set of RPCs, co-expressing the POU Class 4 Homeobox 1 and 2 (Pou4f1/Brn3a and Pou4f2/Brn3b) and contributing to the generation of RGCs (Hufnagel et al., 2010; Brzezinski et al., 2011). Interestingly, knocking down the expression of Pou4f2/Brn3b in MGCs cultured in conditions to induce stem cell-like properties hampers the differentiation into RGCs (Singhal et al., 2012; Song et al., 2013; Wu et al., 2016).

Here we report that forced expression of NEUROG2 is sufficient to convert postnatal rodent MGC into a neurogenic state. Either ASCL1 or NEUROG2 elicited induced neurons (iNs) that express genes of bipolar, horizontal and amacrine cells, as well as photoreceptors. However, only forced expression of NEUROG2 led to the generation of iNs expressing hallmarks

of RGCs. We also show that treatment with epidermal growth factor (EGF) and basic fibroblast growth factor (FGF-2) during the expansion of MGCs affects lineage-conversion efficiencies and iN-fate specification. Finally, we provide evidence for an instructive role of NEUROG2 in the specification of RGC fate in late retinal progenitors that are not competent to generate this cell type *in vivo* (Young, 1985; Turner et al., 1990; Rapaport et al., 2004; He et al., 2012). Collectively, our results indicate that NEUROG2 can regulate the specification program of both late retinal progenitors and MGC to generate RGCs, and, therefore, might be an interesting candidate for gene-based therapies to treat retinal degenerations.

## MATERIALS AND METHODS

### Animals

C57BL/6 mice were obtained from the Biotério Setorial do Instituto do Cérebro (BISIC). All experiments were approved by and carried out in accordance with the guidelines of the Institutional Animal Care and Use Committee of the Federal University of Rio Grande do Norte (license number #048/2014).

### Müller Glial Cell (MGC) Culture

MGCs were purified from postnatal day (P)7-9 mice according to previously described protocols (de Melo Reis et al., 2008). Briefly, retinas were dissected out and chemically dissociated with TrypLE (Life Technologies) for 10 min at 37°C. Isolated cells were counted using a Neubauer chamber and plated onto T75 culture flasks with DMEM F12 (Gibco) plus 10% fetal bovine serum (Gibco), 3.5 mM glucose (Sigma), 4.5g/L GlutaMax (Gibco), 100 U/mL penicillin/streptomycin (Gibco), either with or without 10 ng/mL of epidermal growth factor (EGF, Gibco) and 10 ng/mL of fibroblast growth factor 2 (FGF2, Gibco). Half of the medium was changed once a week during the period of MGCs expansion.

### Plasmids

Plasmids contain the internal chicken  $\beta$ -actin promoter fused with a cytomegalovirus enhancer (pCAG), the coding sequence for either Ascl1 or Neurog2, an internal ribosomal entry site (I) and coding sequences for either DsRed or GFP (pCAG-Ascl1-I-DsRed, pCAG-Neurog2-I-DsRed and pCAG-Neurog2-I-GFP). Control plasmids encode only DsRed or GFP (pCAG-I-DsRed or pCAG-I-GFP).

Plasmid stocks were prepared in *Escherichia coli* and purified using an endotoxin-free Maxiprep plasmid kit (Invitrogen). DNA concentration was adjusted to 1  $\mu$ g/ $\mu$ L in endotoxin free TE buffer, and plasmids were stored at  $-20^{\circ}\text{C}$ .

### Nucleofection

After confluence, MGCs were chemically detached from T75 culture flasks with TrypLE enzyme at 37°C, and  $\sim 3 \times 10^5$  cells were mixed with P3 solution (Lonza) and 1  $\mu$ g of plasmids encoding for either NEUROGENIN2 (pCAG-Neurog2-IRES-DsRed) or ASCL1 (pCAG-Ascl1-IRES-DsRed) or only reporter protein DSRED (pCAG-IRES-DsRed). These solutions were placed in a special cuvette and electroporated using Nucleofector

4D (Lonza) with the P3 primary cell program. Next,  $8 \times 10^4$  cells were plated onto glass-coverslips (100013-Knittel) previously coated with laminin (L2020-SIGMA) and Poly-D lysine (Sigma) containing pre-warmed DMEM F12, 10% fetal bovine serum, 3.5 mM glucose, 4.5g/L GlutaMax and 100U/mL penicillin/streptomycin. After 24h, medium was replaced with differentiation medium containing DMEM F12, 3.5 mM glucose, 4.5 g/l GlutaMax, 100 U/ml penicillin/streptomycin and 2% B27 (Gibco).

### **In vivo Electroporation**

*In vivo* electroporation was performed as previously described (Matsuda and Cepko, 2004, 2007). Briefly, P0 Lister hooded rats were anesthetized by placing on ice. One microliter of DNA mix (6.5  $\mu\text{g}/\mu\text{L}$ ) containing 0.1% Fast Green dye (Sigma) prepared in HBSS saline was injected into the subretinal space with a Hamilton syringe equipped with a 33G blunt end needle. Five 99 V pulses were administered for 50 ms at 950 ms intervals, using a forceps-type electrode (Nepagene, CUY650P7) with Neurgel (Spes Medica). The electrodes were oriented such that the positive pole electrode was placed over the injected eye and the negative pole electrode was placed over non-injected eye to ensure that the electrical field is oriented correctly to drive the injected DNA solution from the subretinal space into progenitors. Fast Green in the DNA mix is an injection tracer, which facilitates observation of the spread of the injection solution into the subretinal space (de Melo and Blackshaw, 2018). In addition, the efficiency of electroporation was verified 10 days after electroporation when GFP positive cells were observed in freshly dissected retinas. Retinas were then fixed by immersion in 4% paraformaldehyde in PBS for 16 h. Serial transversal sections of cryoprotected material (10  $\mu\text{m}$ ) were mounted on either Poly-L-lysine (300  $\mu\text{g}/\text{mL}$ ) or silane (6%, Sigma)-treated microscope slides.

### **Immunocytochemistry**

Cell cultures were fixed in 4% paraformaldehyde (PFA) in PBS for 15 min at room temperature. The cells were incubated overnight at 4°C, with primary antibodies diluted in PBS, 0.5% Triton X-100 and 5% goat serum, washed and incubated for 2 h at room temperature, with species-specific secondary antibodies conjugated to Alexa fluorophores. To stain the nuclei, cells were incubated for 5 min with 0.1  $\mu\text{g}/\text{mL}$  DAPI (4',6'-diamino-2-phenylindone) in PBS 0.1 M. Coverslips were mounted onto glass slides with Aqua Poly/Mount mounting medium (Polysciences, Warrington, PA). Primary antibodies and respective dilutions were: chicken anti-Green Fluorescent Protein (Aves Labs, cat#GFP-1020, 1:1000), rabbit anti-Red Fluorescent Protein (Rockland, cat#600-401-379, 1:1000), mouse anti-microtubule associated protein (Sigma, cat#M1406, 1:500), mouse anti- $\beta$ -III-TUBULIN (TUBB3; Biolegend, cat#MMS-435P, 1:1000), rabbit anti-RBPMS (PhosphoSolutions, cat#1830; 1:100), mouse anti-SYNAPSIN 1 (Synaptic Systems, cat#106001, 1:2000), mouse anti-PARVALBUMIN (SIGMA, cat#p3088, 1:1000), mouse anti-CRALBP (ABCAM, cat# ab15051, 1:500), rabbit anti-GFAP (DakoCytomation, cat#z0334, 1:4000) rabbit anti-SOX2 (ABCAM, cat# ab97959, 1:500), rat anti-BrdU

(ABCAM, cat# ab6326 1:500), rabbit anti-phospho-histone 3 (Millipore, cat#06-570, 1:1000), mouse anti-PAX6 (Millipore, cat#MAB5552, 1:500) and mouse anti-NESTIN (Millipore, cat#mab353, 1:200 millipore).

### **Calcium Imaging**

Calcium imaging was done on MGC cultures at 2–3 weeks post-nucleofection, using Oregon green 488 BAPTA-1 (Invitrogen, 10  $\mu\text{M}$ ). Imaging was performed in a physiological solution containing 140 mM NaCl, 5 mM KCl, 2 mM  $\text{MgCl}_2$ , 2 mM  $\text{CaCl}_2$ , 10 mM HEPES, 10 mM glucose, and 6 mM sucrose, and pH 7.35. Images were acquired every 10 ms with virtually no intervals using a scientific CMOS camera (Andor). The microscope was controlled by Micro-Manager software together with the image processor ImageJ. Changes in fluorescence were measured for individual cells using the time series analyzer plugin v3.0 in ImageJ v1.37. The average of the first ten time-lapse images for each region of interest (ROI) was defined as initial fluorescence ( $F_0$ ), and the variation of fluorescence ( $\Delta F$ ) in each frame ( $n$ ) was calculated as  $F_n - F_0/F_0$ .

### **Quantitative RT-PCR**

MGC cultures were harvested at 13 days after nucleofection, and mRNA was isolated from all cells, including non-transfected MGCs. RNA was extracted using RNeasy Mini Kit (QIAGEN, CA, USA), which includes a genomic DNA elimination step, and the purity and quantity of total RNA was estimated using a ND8000 spectrophotometer (Thermo Scientific NanoDrop Products, DE, EUA). Extractions were carried out of cells from each group (Control, Neurog2 or *Ascl1*), detached chemically with TrypLE and washed with nuclease free PBS, following the manufacturer's protocol. The first-strand cDNA was synthesized using the High-Capacity cDNA Reverse Transcription Kit (Applied Biosystems, NY, USA) in accordance with the manufacturer's instructions, using 900 ng of extracted RNA per sample. Conditions for each cycle of amplification were as follows: 10 min at 25°C; 120 min at 37°C, 5 min at 85°C. The final cDNA products were amplified using RT2 Real-Time SyBR Green/ROX PCR Mix (QIAGEN, CA, USA) in 25  $\mu\text{L}$  of a reaction mixture pipetted into each well of a 96-well in a Mouse RT2 Profiler Custom PCR Array. The array was designed to simultaneously examine mRNA levels of 18 genes commonly expressed in retina cell types (RLBP1, GLUL, NRL, RHO, RCVRN, PDE6G, PROX1, LHX1, VSX2, SLC32A1, TH, CHAT, SLC17A6, POU4F1, CALB2, RBFOX3, SYN1, and PVALB) and 2 housekeeping genes (GAPDH and RPL19), following the manufacturer's protocol. Real-time PCR was performed using a two-step cycling program, with an initial single cycle of 95°C for 10 min, followed by 40 cycles of 95°C for 15 s, then 60°C for 1 min, in an ABI ViiA 7 Real-Time PCR System (Applied Biosystems, NY, USA) with Sequence Detector System software v1.2. The ramp rate was adjusted to 1°C/s following manufacturer's instruction. A first derivative dissociation curve was built (95°C for 1 min, 65°C for 2 min, then ramped from 65°C to 95°C at a rate of 2°C/min). The formation of a single peak at temperatures higher than 80°C confirmed the presence of a single PCR product in the reaction mixture.

For data analysis the  $2^{(-\Delta\Delta Ct)}$  method (Livak and Schmittgen, 2001) was implemented using normalized threshold cycle (Ct) values provided by two independent experiments of nucleofection. Furthermore, we applied experiments using mRNA pool of two independent transfection experiments and used the Ct data to perform normalization and follow the  $2^{(-\Delta\Delta Ct)}$  method (Livak and Schmittgen, 2001), considering the sensitivity, specificity, and reproducibility expected of real-time PCR using RT<sup>2</sup> Profiler PCR Array System from QIAGEN. Endogenous gene control used in the normalization was the average of the mouse GAPDH and RPL19. A positive value indicates gene up-regulation and a negative value indicates gene down-regulation.

To confirm that genes upregulated in MGCs could indicate the acquisition of a retinal neuron-like phenotype in MGC-derived iNs, we performed the same analysis using cerebellum astroglia cell cultures 13 days after nucleofection with either Neurog2 or Ascl1 (Chouchane et al., 2017).

## Bioinformatics

Dataset raw count table and published metadata were obtained from GSE63472 accession code. A modified Seurat pipeline was used to re-analyze single-cell RNAseq data. First, we excluded from our analysis genes that were not expressed in at least 10 cells. Next, we selected cells expressing 500 to 5,000 genes, and <5% of mitochondrial genes ( $n = 21,494$  cells). Metadata variables as number of genes and percentage of mitochondrial expression were also used to regress out some unnecessary clustering bias. Based on *PCElbowPlot*, we used 30 PC's in *FindClusters* (resolution = 2) and *RunTSNE* Seurat's functions. After that, using old assigned clusters and markers found by *FindAllMarkers* function (Macosko et al., 2015), new assigned clusters were labeled. Retinal cell types ( $n = 21,176$  cells) were classified according to the levels of expression of genes in Müller glia cells, astrocytes, amacrine cells, bipolar cells, horizontal cells, cones, rod cells, and ganglion cells (Macosko et al., 2015). Cones and rod cells were merged in a single-group (Photoreceptors).

## Quantifications

To characterize MGC cultures we examined 20 fields at 40 $\times$  magnification for CRALBP and GFAP, and 20 fields at 20 $\times$  magnification for Nestin, Pax6, and PH3 proteins. To quantify the reprogramming process, cells were examined for colocalization of DSRED and TUBB3 immunoreactivity at 13 days post nucleofection (dpn), in 20 fields at 20 $\times$  magnification, and the same was done for MAP2 protein. For all protocols of quantification, we counted immunoreactive cells in 3 independent experiments.

To estimate a neuronal polarization index, we divided the neurons into 4 quadrants and measured the axial distribution of neuronal processes. Nineteen neurons were analyzed for the condition MGC with EGF/FGF + Neurog2, 31 neurons for MGC without + Neurog2, 26 neurons for MGC with EGF/FGF + Ascl1 and 21 neurons for MGC without EGF/FGF + Ascl1.

Distribution of GFP+ cells in the P10 rat retinas following *in vivo* electroporation at P0 in Lister-hooded pups was examined in 26 sections from 5 control-electroporated retinas and 27 sections

from 5 Neurog2-electroporated retinas. The outer nuclear layer (ONL), inner nuclear layer (INL), and ganglion cell layer (GCL) were identified using DAPI counter-staining. MGCs were identified by their radial morphology and expression of CRALBP.

## Statistical Analysis

All statistical data are presented as the mean  $\pm$  standard error of the mean (SEM) of at least three independent experiments. Statistically significant differences were assessed using unpaired *t*-test, one-way or two-way analysis of variance (ANOVA). Confidence interval is 95%.

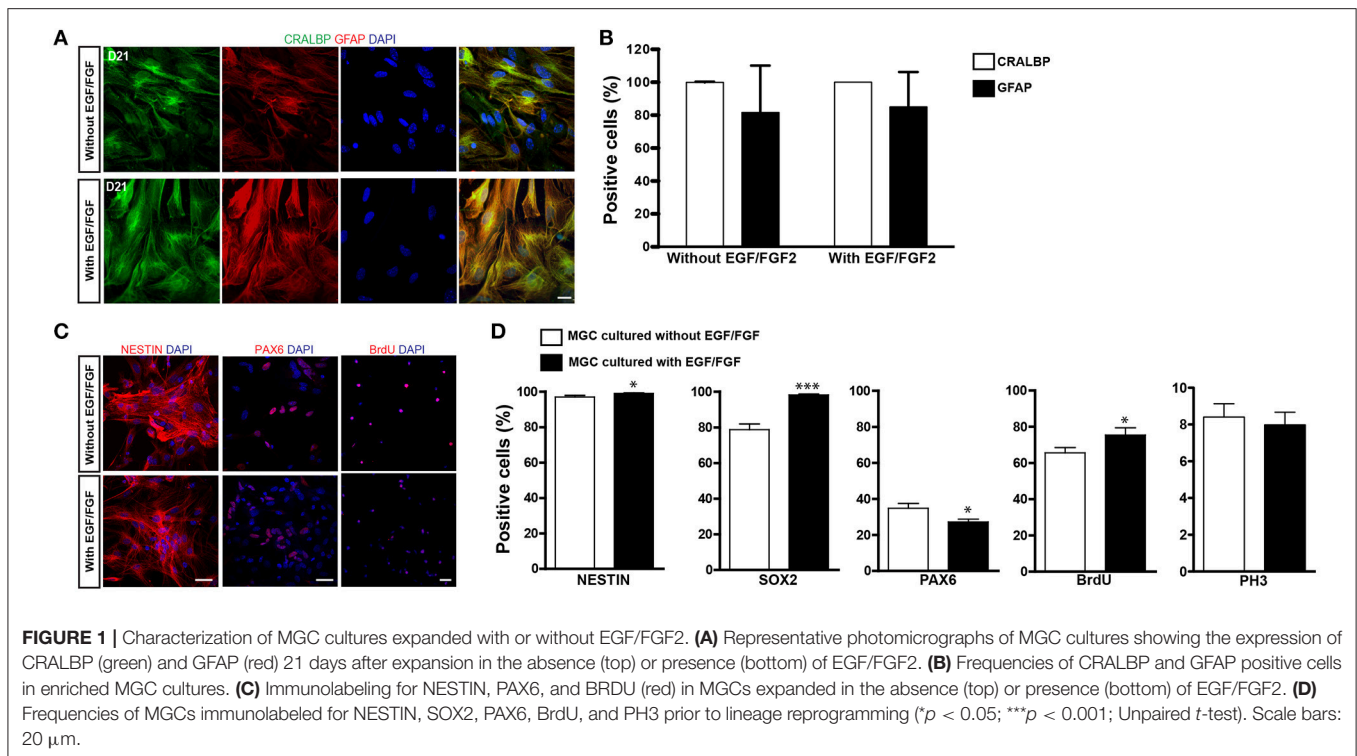
## RESULTS

### Properties of Cells Expanded in the Presence or Absence of EGF/FGF2

Enrichment of MGCs was done according to a previously described method (Hicks and Courtois, 1990). Using this method we (de Melo Reis et al., 2008) and others (Das et al., 2006) have shown that virtually all cells after 2–3 weeks in culture express the MGC markers vimentin, glutamine synthetase (GS), cellular retinaldehyde-binding protein (CRALBP). Based on the previously reported use of selected growth factors to expand astroglial populations for lineage reprogramming into iNs (Berninger et al., 2007; Heinrich et al., 2010; Chouchane et al., 2017), we cultured cells either with or without EGF/FGF2. After expansion, virtually all cells in cultures obtained using both protocols expressed the MGC protein CRALBP (**Figures 1A,B**). A high percentage of cells also expressed glial acid fibrillary protein (GFAP), which is upregulated in MGC cultures (Das et al., 2006). No significant difference was observed between the two expansion conditions (**Figures 1A,B**).

MGCs and late-progenitors in the retina share the expression of several proteins, including NESTIN, sex determining region Y (SRY)-box 2 (SOX2) and Paired box 6 [PAX6; (Karl et al., 2008; Lin et al., 2009; Bhatia et al., 2011)], what has led to the suggestion that MGCs may have neural stem cell-like properties (Das et al., 2006; Lawrence et al., 2007; Nickerson et al., 2008; Giannelli et al., 2011). Accordingly, we found that more than 97% of cells expressed NESTIN and this percentage was slightly increased in the presence of EGF/FGF2 (**Figures 1C,D**;  $97.02 \pm 0.95\%$  vs.  $99.05 \pm 0.32\%$ ,  $p = 0.0466$ , unpaired *t*-test.  $N = 3$  independent experiments). Similarly, expression of SOX2 was also higher among MGCs expanded in the presence of EGF/FGF2 (**Figure 1D**;  $78.71 \pm 3.21\%$  vs.  $98.20 \pm 0.48\%$ ,  $p < 0.0001$ , unpaired *t*-test.  $N = 3$  independent experiments). In contrast, the proportion of MGCs expressing PAX6 was higher in the absence of EGF/FGF2 (**Figures 1C,D**;  $34.87 \pm 2.60\%$  vs.  $27.20 \pm 1.58\%$ ,  $p = 0.013$ , unpaired *t*-test.  $N = 3$  independent experiments).

To examine the proliferative potential of enriched MGCs, we added the thymidine analog BrdU to the cultures at day 20. The percentage of MGCs labeled with BrdU (BrdU+) after 36 h of incubation was slightly higher with, rather than without EGF/FGF2 (**Figures 1C,D**;  $65.54 \pm 2.97\%$  vs.  $75.41 \pm 3.94\%$ ,  $p = 0.047$ , unpaired *t*-test.  $N = 3$  independent experiments). However, the percentage of phospho-histone labeled (PH3+) mitotic MGCs was similar in both conditions (**Figure 1D**; 8.40



$\pm 0.72\%$  vs.  $7.98 \pm 0.69\%$ ,  $p = 0.70$ , unpaired  $t$ -test.  $N = 3$  independent experiments), which could be explained by a selective lengthening of the S-phase upon EGF/FGF2 treatment. Collectively, these observations support the interpretation that cells enriched in our cultures are presumptive MGCs that retain some properties observed in late-progenitors of the developing retina. However, we never observed spontaneous neurogenesis in these cultures, suggesting that a potential progenitor state of presumptive MGCs in culture is associated with a glial-fate restriction.

### Expression of Either NEUROG2 or ASCL1 Is Sufficient to Convert MGCs Into iNs

Next, we tested whether the expression of NEUROG2 may reprogram enriched MGCs into iNs, as compared with ASCL1 as previously described (Pollak et al., 2013). Expanded MGCs were harvested and transfected with control-I-GFP, Neurog2-I-GFP (Figure 2B), Neurog2-I-DsRed (Figures 2D,F) or Ascl1-I-DsRed plasmids (Figures 3A,C), and maintained for 13 days (1 day in growth medium + 12 days in differentiation medium; Figure 2A). At the end of this period, cells transfected with control plasmids maintained both their typical glial morphology and the content of the glia-specific protein GFAP (Figure 2C). In contrast, a substantial fraction of NEUROG2-containing cells underwent robust morphological changes, characterized by reduction of the cell body and extension of thin and long primary processes (usually 2 or 3) with small ramifications, similar to the morphology of neuronal cells in culture (Figures 2B,D,F). Accordingly, these cells also contained the neuron-specific proteins TUBB3 (Figure 2D) and microtubule associated protein

2 (MAP2) (Figure 2F), indicating that NEUROG2 led to conversion of cultured MGCs into iNs. The frequency of iNs was significantly higher in cultures containing MGCs expanded in the presence, as compared with the absence of EGF and FGF2 ( $71.0 \pm 4.1$  vs.  $26.4 \pm 5.1\%$ ;  $p < 0.001$ ; Tukey's multiple comparison test; Figure 2E), suggesting that these growth factors facilitate reprogramming. Additionally, about 90% of iNs also expressed MAP2 (Figures 2F,G) independently of mitogenic factors during enrichment, further suggesting the acquisition of a neuronal phenotype.

Lentiviral-mediated expression of ASCL1 reportedly induced the conversion of about 30% of cultured MGCs into neuronal-like cells (Pollak et al., 2013). In our model, nucleofection of ASCL1 led more than half of cultured MGCs to convert into iNs (Figures 3A,B). The proportion of iNs was higher among MGCs previously expanded in the presence, rather than in the absence of EGF and FGF2 ( $68.1 \pm 4.9$  vs.  $53.7 \pm 5.5\%$ ;  $p < 0.05$ ; Tukey's multiple comparison test; Figure 3B), and 97% of iNs also expressed MAP2 (Figure 3D). Collectively, our data indicate that the expression of either NEUROG2 or ASCL1 is sufficient to lineage-reprogram MGCs into iNs, as well as that previous exposure of MGCs to EGF and FGF2 facilitates reprogramming.

### Functional and Morphological Differentiation of MGC-Derived iNs

To evaluate whether iNs derived from lineage reprogrammed cultured MGCs develop features of mature functional neurons, we performed calcium imaging using a genetically encoded calcium indicator (GCAMP5) and a fluorescent dye (Oregon green BAPTA-1). MGC cultures nucleofected with either Ascl1

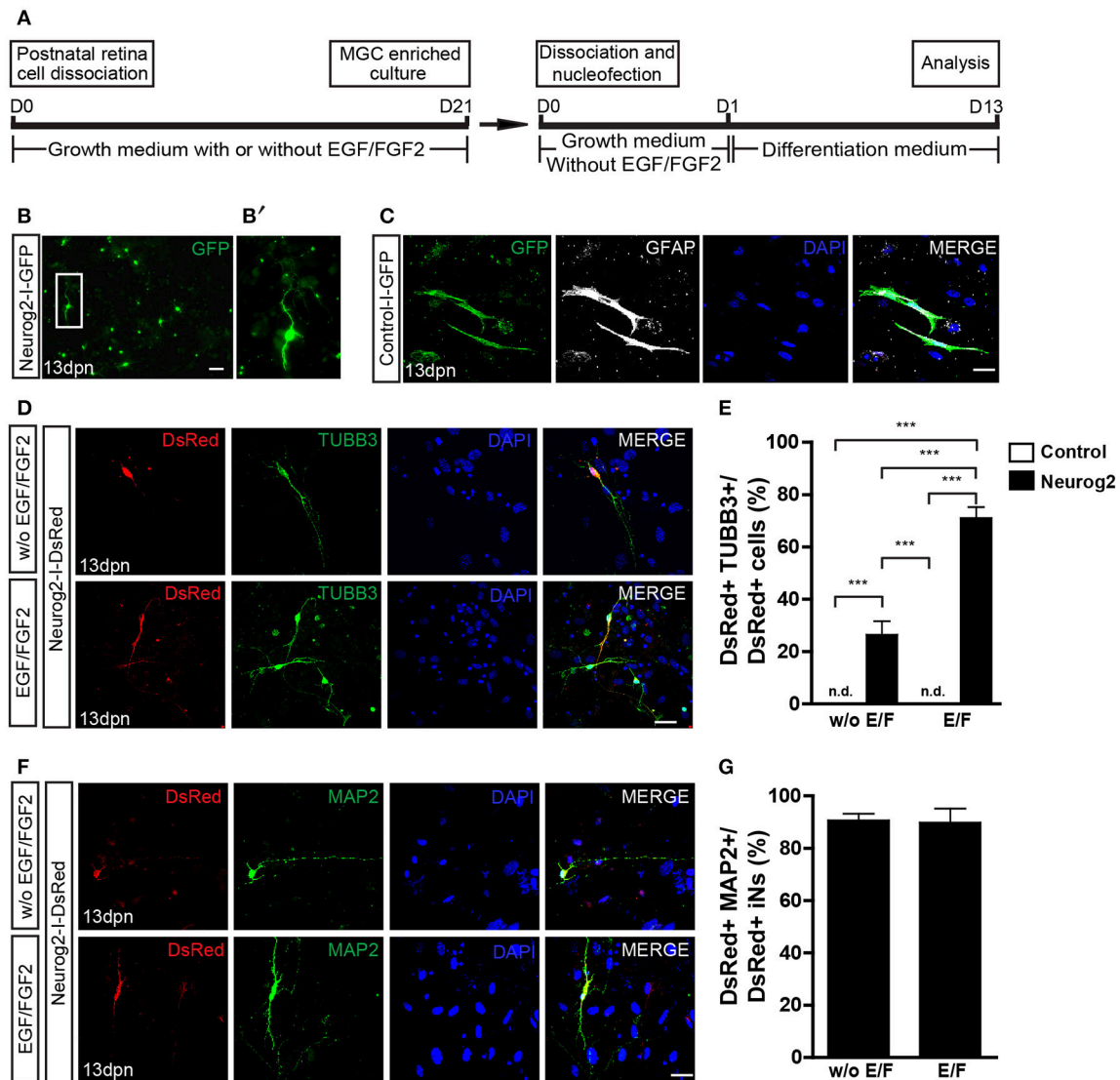


**FIGURE 2** | Expression of NEUROG2 converts MGCs into iNs. **(A)** Experimental design. Note that EGF/FGF2 are used only during MGC expansion. **(B–B')** Overview of MGC cultures 13 days post nucleofection (dpn) with Neurog2-I-GFP showing the presence of GFP+ cells (green) adopting a neuronal-like morphology (white inset, magnified in **B'**). **(C)** Representative photomicrographs of MGC cultures at 13 dpn with control-I-GFP, showing GFP+ cells (green) that maintain glial morphology and contain GFAP (white). **(D)** Immunolabeling of the neuronal protein  $\beta_{III}$ -TUBULIN (TUBB3, green) in DsRed (red) cells at 13 dpn with Neurog2-I-DsRed in MGCs cultures expanded either without (top) or with (bottom) EGF/FGF2. **(E)** Frequencies of DsRed+/TUBB3+ iNs amongst total DsRed+ cells at 13 dpn ( $***p < 0.001$ ; Tukey's multiple comparison test). **(F)** Immunolabeling for the neuronal protein MAP2 (green) in DsRed (red) cells at 13 dpn with Neurog2-I-DsRed in MGCs expanded either without or with EGF/FGF2. **(G)** Frequencies of DsRed+MAP2+ iNs amongst all DsRed+ iNs. Photomicrographs in **(C,D,F)** are single confocal Z stacks. Nuclei are stained with DAPI (blue). Scale bars: 20  $\mu$ m.

or Neurog2 expression plasmids were maintained for 15 days, and then treated with Oregon green BAPTA (see Materials and Methods). Fast fluctuations of intracellular calcium levels leading to sudden fluorescence changes, likely produced by an abrupt aperture of voltage-gated calcium channels mediated by synaptic activity (Bonifazi et al., 2009; Yang and Yuste, 2017), were detected in more than half of iNs (Neurog2 with EGF/FGF2: 12/20; Neurog2 without EGF/FGF2: 13/18; and Ascl1 with EGF/FGF2: 11/20; Ascl1 without EGF/FGF2: 12/19) (**Figure 4**

and **Supplementary Videos**). In contrast, non-transfected MGCs showed slow calcium fluctuations (**Figure 4**).

We also examined the morphology of MGC-derived iNs in the various experimental groups (**Figure S1**). Expression of either Neurog2 or Ascl1 leads to the generation of diverse iNs (**Figures S1A,B**). Notwithstanding, whereas three-quarters of Neurog2-converted iNs were either unipolar or bipolar, Ascl1-converted iNs had approximately equal proportions of either multipolar or uni/bipolar morphologies (**Figure S1C**). These

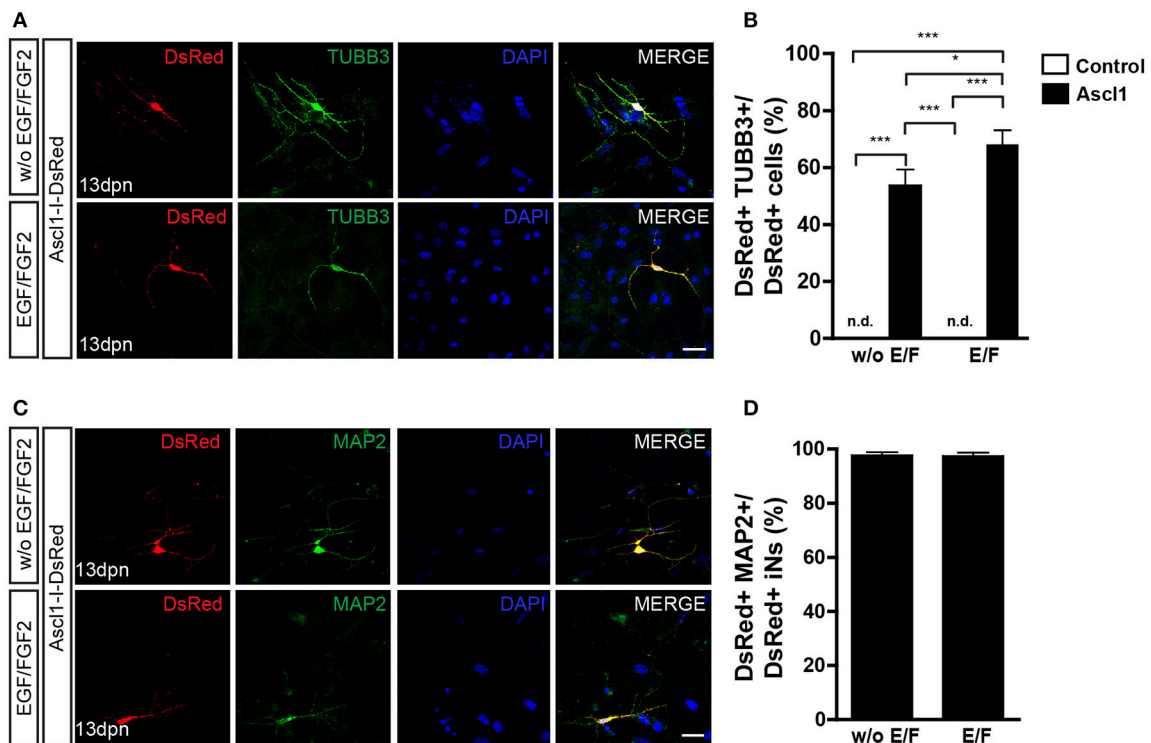


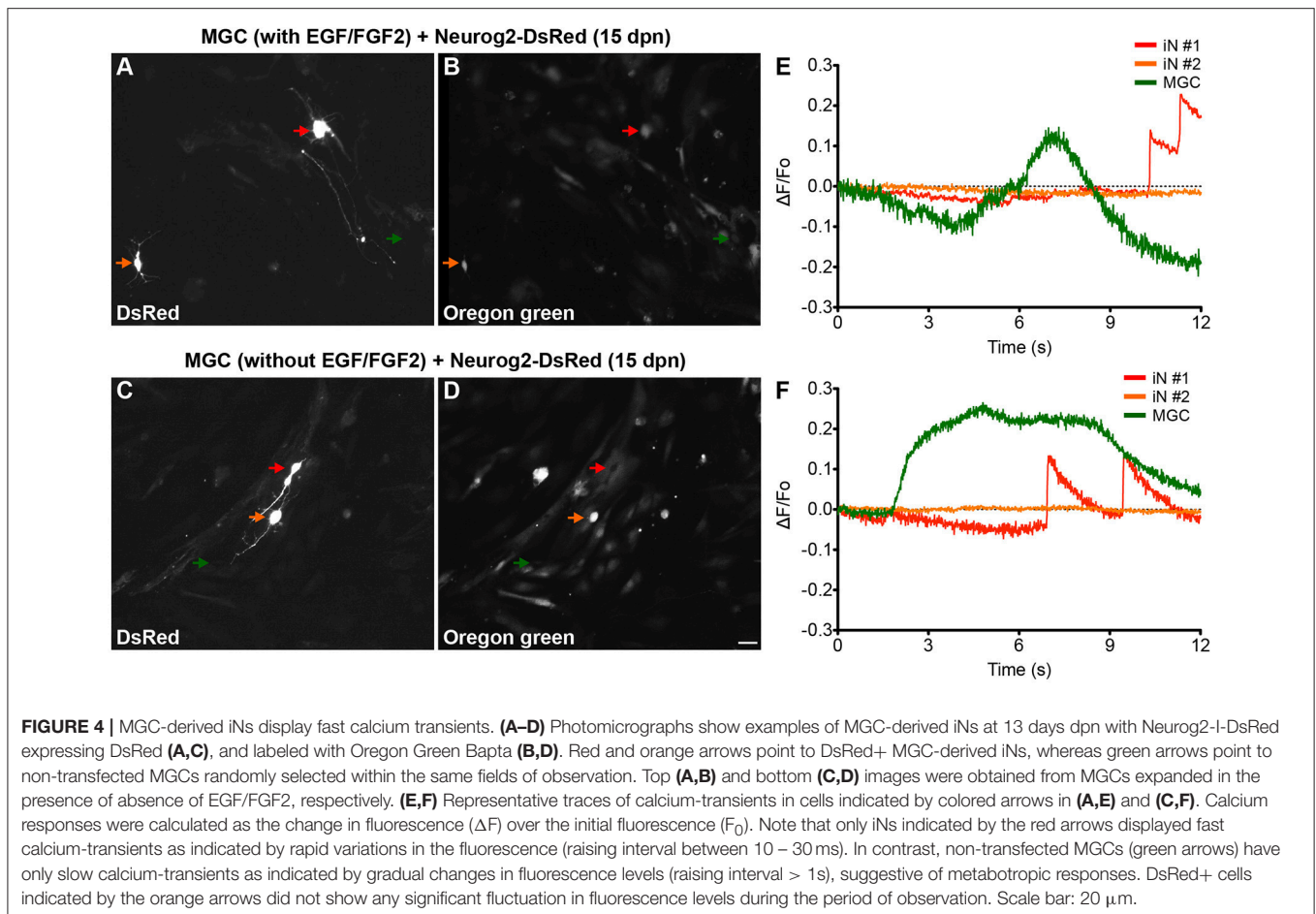
**FIGURE 3** | Expression of ASCL1 converts MGCs into iNs. **(A)** Representative photomicrographs of MGC cultures expanded without or with EGF/FGF2 at 13 dpn with Ascl1-I-DsRed, showing DsRed+ cells (red) immunolabeled for  $\beta_{III}$ -TUBULIN (TUBB3, green) **(B)** Frequencies of DsRed+/TUBB3+ iNs amongst total DsRed+ cells at 13 dpn (\* $p < 0.05$ ; \*\*\* $p < 0.001$ ; Tukey's multiple comparison test). **(C)** Immunolabeling of the neuronal protein MAP2 (green) in DsRed (red) cells at 13 dpn with Ascl1-I-DsRed in MGCs expanded without or with EGF/FGF2. **(D)** Frequencies of DsRed+MAP2+ iNs amongst all DsRed+ iNs. Photomicrographs in **(A,C)** are single confocal Z stacks. Nuclei are stained with DAPI (blue). Scale bars: 20  $\mu$ m.

observations suggest that Neurog2 and Ascl1 iNs may acquire distinct phenotypes.

## MGC-Derived iNs Express Key Genes of Retinal Neurons

It has been suggested that the origin of reprogrammed astroglial cell lineages affects the phenotype of induced neurons (Chouchane et al., 2017). We tested whether MGC-derived iNs show hallmarks of bona fide retina neurons, after lineage conversion induced by either ASCL1 or NEUROG2 (Figure 5). First, we took advantage of single-cell transcriptomes available in the literature (Macosko et al., 2015) to identify molecular signatures of the major retinal cell types (Figure 5A and Figure S2). Based on single-cell RNA sequence of adult mouse retina cells (Macosko et al., 2015), we defined a small set of transcripts with enriched expression in MGCs (RLBP1 and GLUL), astrocytes (GFAP), photoreceptors (NRL, RHO, RCVRN, and PDE6G), horizontal cells (PROX1 and LHX1), bipolar cells (VSX2), amacrine cells (PAX6, SLC32A1, GAD1, GAD2, TH, and CHAT) and RGCs (RBPMS, SLC17A6, POU4F1, CALB2, RBFOX3, SYN1, TUBB3, and PVALB). Next, we used qRT-PCR to compare the expression of these molecular markers in MGC cultures expanded in the presence or absence of EGF/FGF2, and nucleofected with either Neurog2 or Ascl1

(Figures 5B,C). Despite the small number of iNs amongst the total population of MGCs (~1–2%), we detected an increase in the expression of several genes commonly expressed by retina neurons in MGC cultures nucleofected with Neurog2 or Ascl1 (Figures 5B, C), but not among cerebellum astroglial cells nucleofected with the same plasmids (Figure S3), which are known to adopt mostly a GABAergic iN phenotype (Chouchane et al., 2017). Interestingly, differences were observed among cells converted through each of the two expansion protocols. While MGC-derived iNs, induced by expression of either ASCL1 and NEUROG2 grown in the absence of EGF/FGF2 upregulated key genes of photoreceptors, genes of amacrine cells were expressed only in iNs derived from MGCs expanded in the presence of growth factors. In contrast, increased levels of genes commonly expressed by horizontal and bipolar cells were detected in all experimental conditions. Surprisingly, we also found that many genes commonly expressed by RGCs were upregulated in MGC-derived iNs, in particular the specific RGC genes SLC17A6 and POU4F1 (Quina et al., 2005; Martersteck et al., 2017), but the same was not observed in cerebellar astroglia-derived iNs (Figure S3). This effect was much more robust after expression of NEUROG2 (Figure 5B), independently of the expansion protocol. Altogether, the transcriptome panel suggests that either Neurog2 or Ascl1 may induce distinct, but



partly overlapping retina neuronal phenotypes in MGC-derived iNs, but Neurog2 seems to induce a more complete RGC-like phenotype.

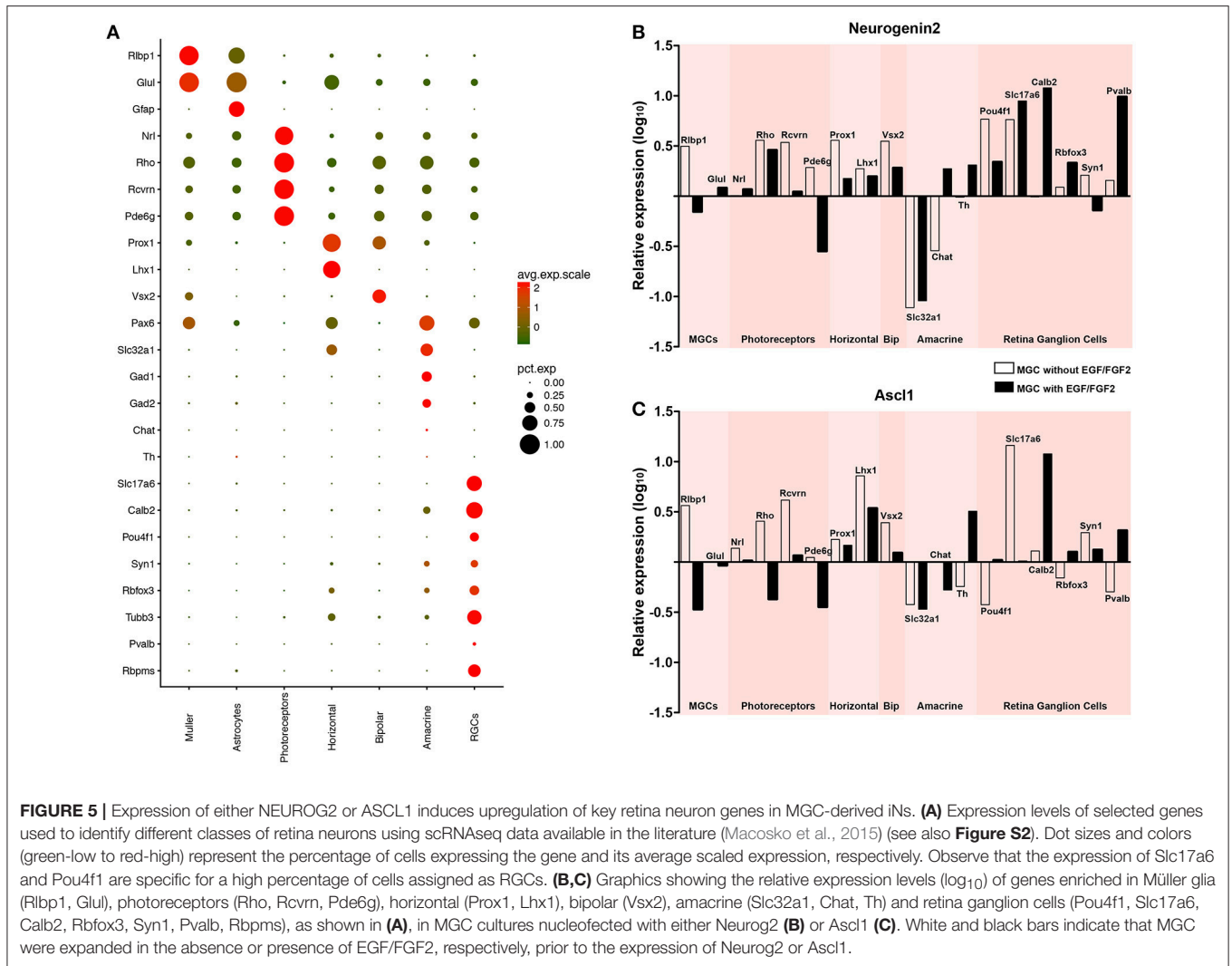
### Neurog2-Induced RGC-Like Phenotypes

To further test for the acquisition of RGC features by MGC-derived iNs, we immunolabeled markers of retina neurons in individual iNs (**Figure 6**). NEUROG2-converted neurons contained RNA Binding Protein mRNA Processing Factor (RBPMS; **Figures 6A–C**), a selective marker of RGCs in the mammalian retina (Rodríguez et al., 2014), as well as TUBB3 (**Figures 2, 6D–F**), PARV (**Figures 6G–I**) and SYN1 (**Figures 6J–L**), all of which are enriched in RGCs *in vivo* (**Figure 5A**). These findings, together with the qRT-PCR data, support the interpretation that NEUROG2 is sufficient to induce a RGC-like phenotype in MGC-derived iNs.

### Overexpression of NEUROG2 Resumes RGC Generation in the Neonatal Retina *in vivo*

Finally, we tested whether the expression of NEUROG2 in late retinal progenitors induces *de novo* generation of RGCs. To that

effect, sub-retinal injections of either pCAG-I-GFP or pCAG-Neurog2-I-GFP plasmids were followed by electroporation in P0 rats (**Figure 7**). Late progenitors are transcriptionally similar to MGCs and also have restricted neurogenic potential (Cepko, 1999; Blackshaw et al., 2004; Ooto et al., 2004; Jadhav et al., 2009; Nelson et al., 2011; He et al., 2012; Karl and Reh, 2012; Löffler et al., 2015). Both late progenitors and MGCs are not competent to generate RGCs in the rodent retina. As previously described (Matsuda and Cepko, 2004), 10 days after *in vivo* electroporation the vast majority (~80%) of GFP+ cells in control-electroporated retinas settled in the outer nuclear layer (ONL) and differentiated into rod cells, while the remaining cells located mostly in the inner nuclear layer (INL) and differentiated into bipolar, MGCs or amacrine cells (**Figures 7A,E**). Also consistent with the literature (Matsuda and Cepko, 2004), a negligible number of GFP+ cells was found in the ganglion cell layer (GCL) of control-electroporated animals (2 cells in one animal out of 1,254 GFP+ cells counted from 5 animals— $26 \times 250 \mu\text{m}$  sections), whereas a significant proportion of cells in all animals displayed radial morphologies and expressed CRALBP (**Figure S4**), indicating the acquisition of a MGC phenotype ( $10.71 \pm 0.69\%$ ,  $n = 5$  animals, 1,487 GFP+ cells). In sharp contrast, in retinas electroporated with pCAG-Neurog2-I-GFP plasmid, we failed to detect any cell with a radial morphology or expression of CRALBP (1,340

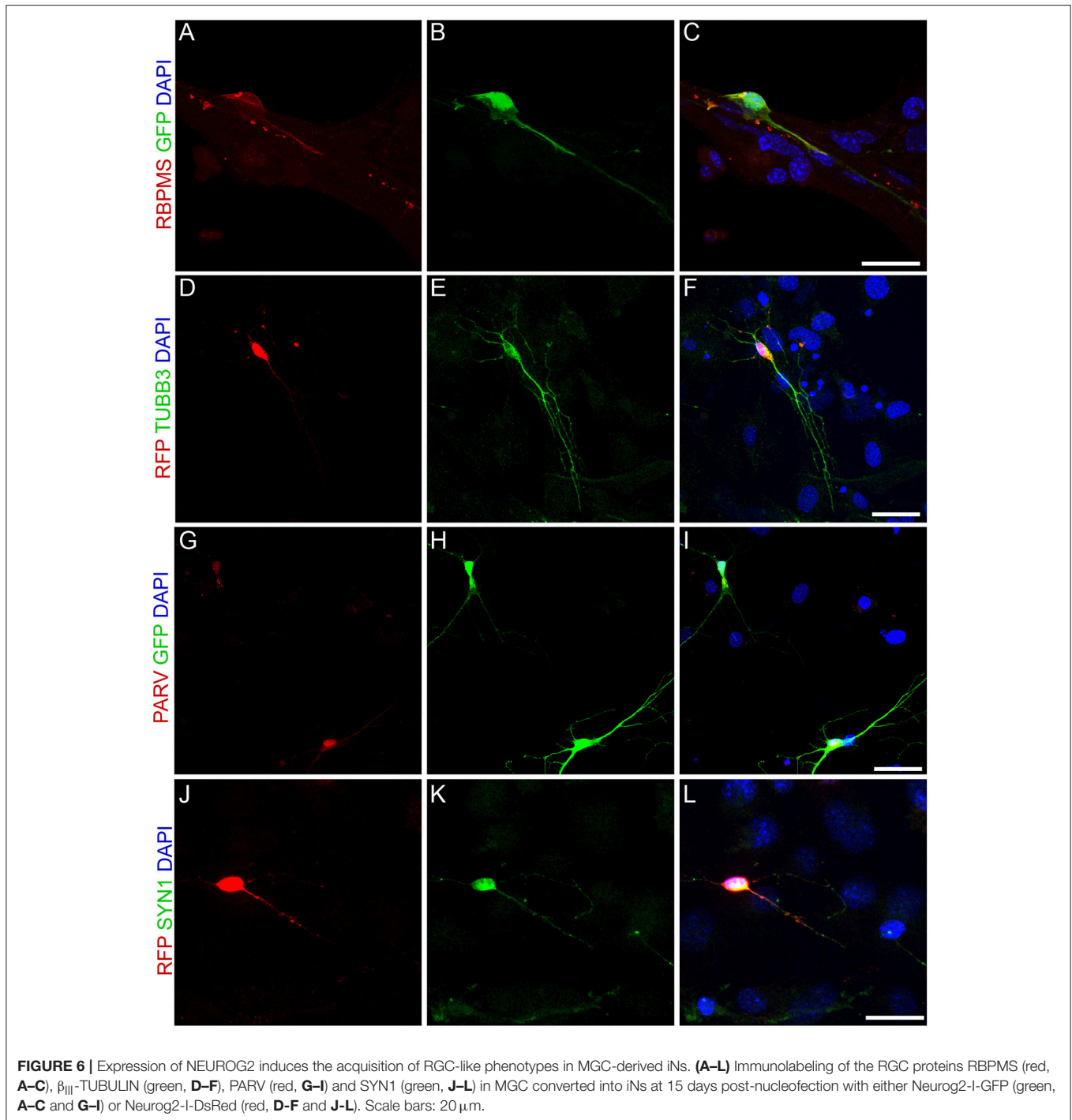


GFP+ cells analyzed from 5 animals). About 65.5% of GFP+ cells settled in the ONL and 33% in the INL, but a significant fraction (17 cells in 5 animals out of 1340 GFP+ cells counted from 5 animals— $27 \times 250 \mu\text{m}$  sections) of cells was found in the GCL (**Figures 7C–I**). Quantification of the number of GFP+ cells in  $250 \mu\text{m}$  of 27 sections of 5 retinas showed that the mean number of GFP+ cells in the GCL was significantly increased in Neurog2-electroporated animals as compared to controls, suggesting that NEUROG2 expression resumed the generation of RGCs (**Figure 7F**). Accordingly, we also found that GFP+ cells in the GCL expressed classical markers of RGCs, such as RBPMS (**Figures 7G–I**) and TUBB3 (**Figure S5**) and extended thin axonal processes that reached the optic nerve (**Figure 7J**). Some GFP-expressing cells within the GCL also extended processes toward the inner plexiform layer, consistent with the morphology of RGCs (**Figures 7G, 8**). Moreover, GFP+ cells within the GCL also displayed varied patterns of dendrite stratification (**Figure 8**), consistent with distinct RGC morphologies in the rodent retina (Sanes and Masland, 2015). Altogether, these data support the hypothesis that the expression of NEUROG2 endows

late retinal progenitors with the potential to generate RGCs, while it inhibits the differentiation of MGCs *in vivo*.

## DISCUSSION

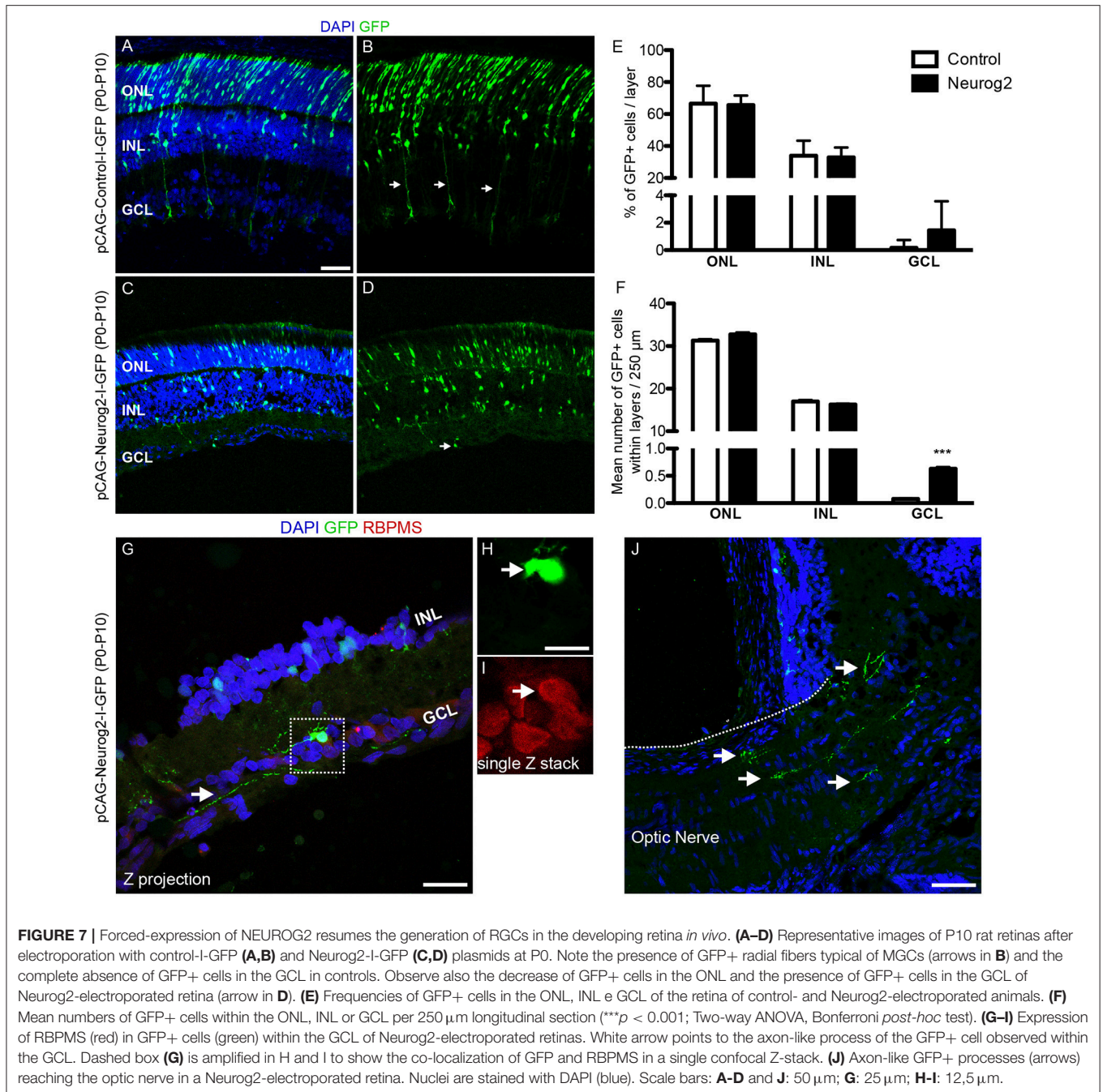
Here we show that cells isolated in culture and expressing several hallmarks of Müller cells, the main type of glia found in the vertebrate retina, can be reprogrammed into neurons when transduced with plasmids encoding either of the basic Helix loop Helix (bHLH) transcription factors Neurog2 or Ascl1. Cell-lineage reprogramming is affected by treatment with EGF and FGF2 during MGC enrichment, and led to the expression of typical neuronal markers, MAP-2 and TUBB3. Induced neurons expressed clusters of genes consistent with the profile of retinal cells, suggesting that distinct retinal neuron phenotypes are elicited in MGC-derived iNs. Notably, only iNs generated after expression of NEUROG2 upregulated a set of genes compatible with the acquisition of a possible RGC identity. A role for NEUROG2 in the induction of RGC fate was also



observed in late progenitors of the neonatal mouse retina *in vivo*, suggesting that Neurog2 is a good candidate for gene therapies aiming at the regeneration of RGCs in the adult injured retina.

Lineage reprogramming of astroglial cells into neurons has been heralded as a possible treatment for degenerative or traumatic brain disorders, and recent studies showed evidence of conversion of glial cells into functional neurons with high

efficiency in the murine brain, induced by virally delivered transcription factors (Torper and Gotz, 2017). Astroglial cells isolated from the postnatal rodent cerebral cortex (Berninger et al., 2007; Heinrich et al., 2010) and cerebellum (Chouchane et al., 2017), as well as retinal MGCs (Singhal et al., 2012; Pollak et al., 2013; Song et al., 2013; Ueki et al., 2015; Wu et al., 2016; Jorstad et al., 2017) have been reprogrammed into neurons.



Lentiviral gene transfer of the proneural factor *Ascl1* partially reprogrammed P11/12 Müller glial cells *in vitro* into retinal progenitors 3 weeks after infection (Pollak et al., 2013), a process facilitated by microRNA miR-124-9-9\* (Wohl and Reh, 2016). Combination of *Ascl1* and miR-124-9-9\* led to a peak of 50–60% reprogrammed iNs, whereas *Ascl1* alone reached 30–35% (Wohl and Reh, 2016). The latter is lower than what we found following expression of *Ascl1*, which may be due to the earlier age of the mice from which cells were isolated in our study (P7-9). Indeed, in our hands, MGCs isolated from P21 retina

failed to reprogram into iNs upon expression of either *ASCL1* or *NEUROG2* (data not shown), similar to what has been described for astroglia isolated from the adult mouse cerebral cortex (Heinrich et al., 2010) or even for astroglia isolated from the postnatal cerebral cortex or cerebellum, and maintained in differentiation conditions for several days before *ASCL1* or *NEUROG2* expression (Masserdotti et al., 2015; Chouchane et al., 2017). This resistance to lineage conversion in astrocytes isolated at late developmental stages is likely explained by the epigenetic changes occurring in these cells during differentiation from an

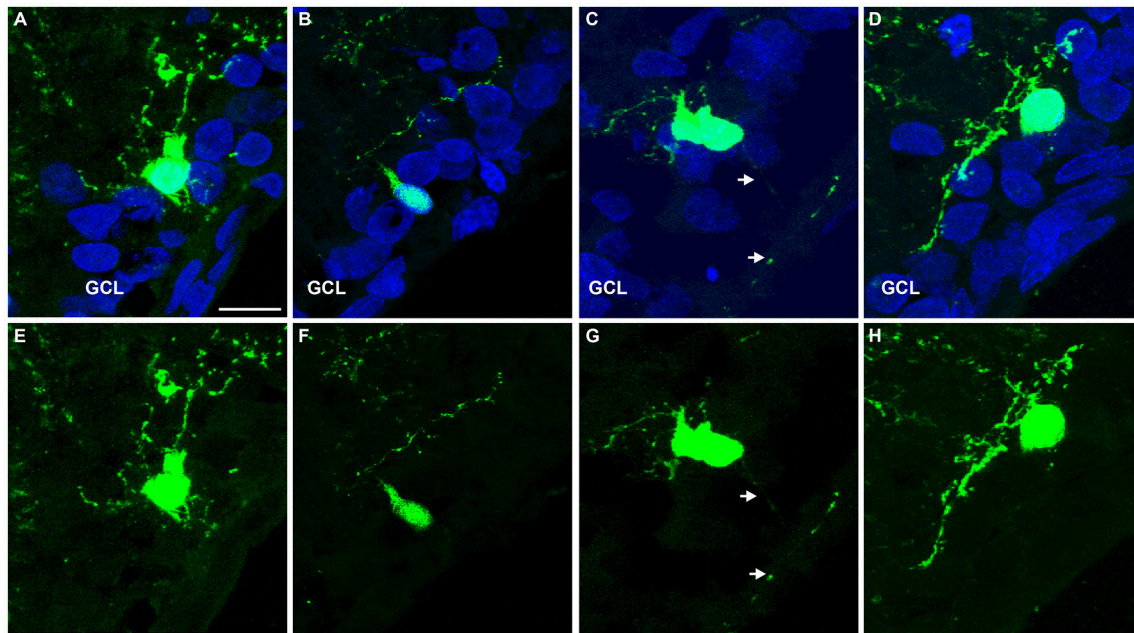


**FIGURE 8** | Representative examples of GFP+ cells within the GCL of Neurog2-electroporated retinas. **(A–H)** Images show GFP+ cells (green) within the GCL of P10 rats after electroporation with Neurog2-I-GFP at P0. Nuclei are stained with DAPI (blue, **A–D**). Note the distinct positions and dendrite stratifications of GFP+ cells (**E–H**), resembling *bona fide* subtypes of rodent RGCs (Sanes and Masland, 2015). Scale bar: 25  $\mu$ m.

immature to mature state (Masserdotti et al., 2015). According to this interpretation, ASCL1-mediated lineage reprogramming of MGCs into iNs in adult mouse retina requires co-treatment with histone deacetylase-inhibitors (Jorstad et al., 2017).

Our data also showed that the presence of mitogenic factors EGF and FGF2 during MGC expansion substantially increased the efficiency of conversion into iNs, suggesting that exposure to those growth factors endows MGCs with higher plasticity. It has been shown that FGF2 induces methylation of Lysine 4 and suppresses methylation of Lysine 9 of histone H3 at the signal transducer and activator of transcription (STAT) binding site (Song and Ghosh, 2004), whereas EGF affects chromatin architecture at the regulatory element of cyclin D1, through a process involving Cre-binding protein (CBP), Histone deacetylase 1 (HDAC1) and Suv39h1 histone/chromatin remodeling complex (Lee et al., 2012). It is conceivable that such effects of EGF/FGF2 upon MGCs may facilitate the binding of NEUROG2 and ASCL1 to their target genes and, therefore, increases the efficiency of conversion. The effect was more pronounced for NEUROG2 than ASCL1; the latter has a known role in the remodeling of the chromatin landscape by itself, which increases its own accessibility to target genes (Raposo et al., 2015). In addition, expression of ASCL1 in NMDA-injured retinas of adult mice was sufficient to lineage reprogram only about 20% of MGCs into Otx2+ neurons, but this effect was enhanced by 2-fold in animals receiving concomitant treatment with trichostatin-A, a potent inhibitor of histone deacetylase (Jorstad et al., 2017).

Alternative explanations for the effects of EGF/FGF2 upon MGC-lineage conversion into iNs are rooted on the roles

of these growth factors in cell proliferation (Todd et al., 2015) and survival (Rolf et al., 2003; Nickerson et al., 2011), dedifferentiation and possibly reprogramming, reviewed in Hamon et al. (2016). Recent work in the adult mouse retina demonstrates that genetic lineage reprogramming of MGCs into photoreceptors *in vivo* requires previous activation of cell proliferation through activation of the beta-catenin pathway (Yao et al., 2018). Here, we observed a larger fraction of NESTIN+, SOX2+, and BrdU+ cells in MGC cultures grown in the presence of EGF/FGF2, suggesting an increase in cell proliferation. However, this effect was much smaller than that observed in lineage-reprogramming efficiencies, indicating that the increased number of iNs observed in cultures treated with EGF/FGF2 cannot be exclusively explained by an increase in MGC proliferation. Thus, the explanation that reprogramming is facilitated by EGF/FGF2 through effects upon chromatin structure remains a likely explanation, although further studies are needed to support this hypothesis.

A critical question in cell reprogramming is whether iNs acquire either single or multiple neuronal phenotypes (Amamoto and Arlotta, 2014; Heinrich et al., 2015). Recent work in our laboratory has shown that the origin of astroglial cells, either from cerebral cortex or cerebellum, affects the phenotype of iNs lineage-converted by either ASCL1 or NEUROG2 (Chouchane et al., 2017). Notably, most iNs generated from astroglia from either cerebellum or neocortex showed central hallmarks of neurons commonly observed in those regions, suggesting that a “molecular memory” in the astroglial cells contributes to the acquisition of specific neuronal phenotypes in iNs (Chouchane and Costa, 2018).

This notion is supported by our current finding that MGC-derived iNs upregulate several genes expressed in retinal neurons. Consistent with previous work (Pollak et al., 2013; Wohl and Reh, 2016; Jorstad et al., 2017), we found that ASCL1-converted MGCs generated iNs which express genes of horizontal and bipolar cells, but few genes commonly observed in photoreceptors, amacrine cells and RGCs, suggesting that these phenotypes are rare and/or incomplete in the converted cells. In contrast, expression of NEUROG2 converted MGCs into iNs accompanied by up-regulation of several genes of photoreceptors, amacrine cells and RGCs. Importantly, the latter phenotype is supported by the expression of two RGC-specific genes, namely Pou4f1 and Scl17a6 (Quina et al., 2005; Martersteck et al., 2017), as well as four other genes highly enriched in RGCs (Syn1, Parv, Calb2 and Tubb3). Immunolabeling confirmed the increased content of three of these markers (TUBB3, SYNAPSIN 1, PARVALBUMIN). Moreover, expression of the selective RGC marker RBPMS (Rodriguez et al., 2014) in MGC nucleofected with Neurog2 further suggests the acquisition of a RGC-like phenotype in iNs. These observations are particularly important, because previous attempts to lineage reprogram MGCs into iNs, both *in vitro* and *in vivo*, have failed to generate iNs with RGC-like phenotypes (Pollak et al., 2013; Wohl and Reh, 2016; Jorstad et al., 2017). Future experiments should address whether the expression of NEUROG2 in MGCs in the intact or injured adult retina are sufficient to lineage convert these cells into RGCs. Nevertheless, our observations in post-natal retinas indicate that NEUROG2 has an important instructive role for the RGC phenotype *in vivo*.

Altogether, our study corroborates previous evidence of the potential of MGC to reprogram into iNs following expression of ASCL1 (Pollak et al., 2013; Wohl and Reh, 2016; Jorstad et al., 2017), and provides compelling evidence that NEUROG2 expression is also sufficient to convert MGCs into iNs expressing several features of RGCs. Our results may thus contribute to develop new strategies of gene therapy aiming at the regeneration of retinal neurons in patients with glaucoma and other neurodegenerative retinopathies.

## AUTHOR CONTRIBUTIONS

All authors reviewed the manuscript. RG and BL contributed to design and perform the experiments, analyzed the data, discussed the results, and prepare figures of the manuscript. DG performed qPCR experiments. DC analyzed single cell RNAseq data. MS conceived electroporation experiments, discussed the results, and contributed to the manuscript. RdMR and RL co-supervised RG's thesis, and contributed to the manuscript. MC provided financial support, directed the project, conceived the experiments, analyzed data, discussed the results, and wrote the manuscript.

## ACKNOWLEDGMENTS

We would like to thank Viviane Valença and Pedro Lucas França for their contribution with *in vivo* electroporation

experiments. This work was supported by Conselho Nacional de Desenvolvimento Científico e Tecnológico (CNPq), Coordenação de Aperfeiçoamento de Pessoal de Nível Superior (CAPES), Fundação de Amparo à pesquisa do Rio de Janeiro (FAPERJ) and Instituto Nacional de Neurociência Translacional (INNT).

## SUPPLEMENTARY MATERIAL

The Supplementary Material for this article can be found online at: <https://www.frontiersin.org/articles/10.3389/fncel.2018.00410/full#supplementary-material>

**Figure S1** | Polarized morphologies are more common in Neurog2- than Ascl1-iNs. **(A)** Morphologies of iNs derived from MGCs nucleofected with either Neurog2 or Ascl1. **(B)** Cartesian plot representing the orientations of primary dendrites in iNs generated in different conditions (Neurog2 without GF = 31 iNs; Neurog2 with GF = 19 iNs; Ascl1 without GF = 21 iNs; Ascl1 with GF = 26 iNs). **(C)** Frequencies of iNs showing unipolar, bipolar, or multipolar morphologies according to the TF used (Neurog2= 50 iNs; Ascl1= 47 iNs). Observe the higher number of uni/bipolar among Neurog2-induced neurons ( $p < 0.05$ ; Chi-square test).

**Figure S2** | Identification of major retina cell types using single-cell transcriptomes. **(A)** Clustering of 21,176 single-cell expression profiles into 39 retinal cell populations using available dataset (Macosko et al., 2015). The plot shows a two-dimensional representation (tSNE) of global gene expression relationships among 21,176 cells. **(B)** Annotation of the same cells into the 7 major retinal cell types, according to the expression of cell-type specific genes. **(C)** List of some differently expressed genes used to classify the 7 major retina cell types and also used to identify the phenotypes of iNs in this study (RT-qPCR and immunocytochemistry).

**Figure S3** | Gene expression in cerebellar astroglia cells nucleofected with Neurog2 or Ascl1. Graphic showing the relative expression levels ( $\log_{10}$ ) of genes used to identify presumptive retina cell phenotypes (**Figure 5**) cerebellar astroglia cell cultures nucleofected with either Neurog2 (white bars) or Ascl1 (black bars). Observe that genes commonly observed in cerebellar neurons (Prox1, Vsx2, Slc32a1, Chat, Rbfox3, and Syn1) are upregulated, whereas genes whose expression is restricted to retinal neurons (Nrl, Rho, Pou4f1, Slc17a6) are not up regulated in cerebellar astroglia-derived iNs.

**Figure S4** | Expression of CRALBP in MGCs generated in the postnatal retina electroporated with control-I-GFP. **(A–C)** Coronal section of a P10 rat retina after electroporation with Control-I-GFP at P0, immunolabeled for GFP (green) and CRALBP (red). Images are single confocal Z-stacks and show the co-localization of GFP and CRALBP in MGC fibers (arrows). Scale bar: 25  $\mu\text{m}$ .

**Figure S5** | Expression of  $\beta_{III}$ -TUBULIN in RGCs generated in the postnatal retina following Neurog2-electroporation. **(A)** Coronal section of a P10 rat retina after electroporation with Neurog2-I-GFP at P0, immunolabeled for GFP (green) and  $\beta_{III}$ -TUBULIN (TUBB3, red). Nuclei are stained with DAPI (blue). Image is a Z-projection of 8 confocal Z-stacks. Dashed box delimits a GFP+ cell within the ganglion cell layer (GCL). **(B,C)** Magnification of the dashed box in A showing the co-localization of GFP and  $\beta_{III}$ -TUBULIN in a single confocal Z-stack. Scale bars: **A:** 50  $\mu\text{m}$ ; **B,C:** 25  $\mu\text{m}$ .

**Supplementary Video 1** | MGC expanded in the presence of EGF/FGF2 and lineage reprogrammed into iNs by NEUROG2 show fast calcium transients. Movie shows 600 frames taken with 10 ms exposure time and no interval. Observe the fast fluorescence intensity increase in the MGC-derived iN indicated by a red arrow in **Figures 4A,B**. MGCs in the same field show slow oscillations in fluorescence.

**Supplementary Video 2** | MGC expanded in the absence of EGF/FGF2 and lineage reprogrammed into iNs by NEUROG2 show fast calcium transients. Movie shows 600 frames taken with 10 ms exposure time and no interval. Observe the fast fluorescence intensity increase in the MGC-derived iN indicated by a red arrow in **Figures 4C,D**. MGCs in the same field show slow oscillations in fluorescence.

## REFERENCES

- Abu-Hassan, D. W., Li, X., Ryan, E. I., Acott, T. S., and Kelley, M. J. (2015). Induced pluripotent stem cells restore function in a human cell loss model of open-angle glaucoma. *Stem Cells* 33, 751–761. doi: 10.1002/stem.1885
- Amamoto, R., and Arlotta, P. (2014). Development-inspired reprogramming of the mammalian central nervous system. *Science* 343:1239882. doi: 10.1126/science.1239882
- Athanasiou, D., Aguila, M., Bevilacqua, D., Novoselov, S. S., Parfitt, D. A., and Cheetham, M. E. (2013). The cell stress machinery and retinal degeneration. *FEBS Lett.* 587, 2008–2017. doi: 10.1016/j.febslet.2013.05.020
- Berninger, B., Costa, M. R., Koch, U., Schroeder, T., Sutor, B., Grothe, B., et al. (2007). Functional properties of neurons derived from *in vitro* reprogrammed postnatal astroglia. *J Neurosci* 27, 8654–8664. doi: 10.1523/JNEUROSCI.1615-07.2007
- Bhatia, B., Singhal, S., Tadman, D. N., Khaw, P. T., and Limb, G. A. (2011). SOX2 is required for adult human muller stem cell survival and maintenance of progenicity *in vitro*. *Invest. Ophthalmol. Vis. Sci.* 52, 136–145. doi: 10.1167/iovs.10-5208
- Blackshaw, S., Harpavat, S., Trimarchi, J., Cai, L., Huang, H., Kuo, W. P., et al. (2004). Genomic analysis of mouse retinal development. *PLoS Biol.* 2:E247. doi: 10.1371/journal.pbio.0020247
- Bonifazi, P., Goldin, M. A., Picardo, M. A., Jorquera, I., Cattani, A., Bianconi, G., et al. (2009). GABAergic hub neurons orchestrate synchrony in developing hippocampal networks. *Science* 326, 1419–1424. doi: 10.1126/science.1175509
- Brzezinski, J. A. T., Kim, E. J., Johnson, J. E., and Reh, T. A. (2011). Ascl1 expression defines a subpopulation of lineage-restricted progenitors in the mammalian retina. *Development* 138, 3519–3531. doi: 10.1242/dev.064006
- Cepko, C. L. (1999). The roles of intrinsic and extrinsic cues and bHLH genes in the determination of retinal cell fates. *Curr. Opin. Neurobiol.* 9, 37–46. doi: 10.1016/S0959-4388(99)80005-1
- Chamling, X., Sluch, V. M., and Zack, D. J. (2016). The potential of human stem cells for the study and treatment of glaucoma. *Invest. Ophthalmol. Vis. Sci.* 57, ORSF11-6. doi: 10.1167/iovs.15-18590
- Chouchane, M., and Costa, M. R. (2018). Instructing neuronal identity during CNS development and astroglial-lineage reprogramming: roles of NEUROG2 and ASCL1. *Brain Res.* doi: 10.1016/j.brainres.2018.02.045. [Epub ahead of print].
- Chouchane, M., Melo De Farias, A. R., Moura, D. M. S., Hilscher, M. M., Schroeder, T., Leao, R. N., et al. (2017). Lineage reprogramming of astroglial cells from different origins into distinct neuronal subtypes. *Stem Cell Rep.* 9, 162–176. doi: 10.1016/j.stemcr.2017.05.009
- Das, A. V., Mallya, K. B., Zhao, X., Ahmad, F., Bhattacharya, S., Thoreson, W. B., et al. (2006). Neural stem cell properties of Muller glia in the mammalian retina: regulation by Notch and Wnt signaling. *Dev. Biol.* 299, 283–302. doi: 10.1016/j.ydbio.2006.07.029
- de Melo Reis, R. A., Cabral-Da-Silva, M., De Mello, F. G., and Taylor, J. S. (2008). Muller glia factors induce survival and neurogenesis of peripheral and central neurons. *Brain Res.* 1205, 1–11. doi: 10.1016/j.brainres.2008.02.035
- de Melo, J., and Blackshaw, S. (2018). *In vivo* electroporation of developing mouse retina. *Methods Mol. Biol.* 1715, 101–111. doi: 10.1007/978-1-4939-7522-8\_8
- Giannelli, S. G., Demontis, G. C., Pertile, G., Rama, P., and Broccoli, V. (2011). Adult human Muller glia cells are a highly efficient source of rod photoreceptors. *Stem Cells* 29, 344–356. doi: 10.1002/stem.579
- Gill, K. P., Hung, S. S., Sharov, A., Lo, C. Y., Needham, K., Lidgerwood, G. E., et al. (2016). Enriched retinal ganglion cells derived from human embryonic stem cells. *Sci. Rep.* 6:30552. doi: 10.1038/srep30552
- Hamon, A., Roger, J. E., Yang, X. J., and Perron, M. (2016). Muller glial cell-dependent regeneration of the neural retina: an overview across vertebrate model systems. *Dev. Dyn.* 245, 727–738. doi: 10.1002/dvdy.24375
- He, J., Zhang, G., Almeida, A. D., Cayouette, M., Simons, B. D., and Harris, W. A. (2012). How variable clones build an invariant retina. *Neuron* 75, 786–798. doi: 10.1016/j.neuron.2012.06.033
- Heinrich, C., Blum, R., Gascon, S., Masserdotti, G., Tripathi, P., Sanchez, R., et al. (2010). Directing astroglia from the cerebral cortex into subtype specific functional neurons. *PLoS Biol.* 8:e1000373. doi: 10.1371/journal.pbio.1000373
- Heinrich, C., Spagnoli, F. M., and Berninger, B. (2015). *In vivo* reprogramming for tissue repair. *Nat. Cell Biol.* 17, 204–211. doi: 10.1038/ncb3108
- Hicks, D., and Courtois, Y. (1990). The growth and behaviour of rat retinal Muller cells *in vitro*. 1. An improved method for isolation and culture. *Exp. Eye Res.* 51, 119–129. doi: 10.1016/0014-4835(90)90063-Z
- Hufnagel, R. B., Le, T. T., Riesenberger, A. L., and Brown, N. L. (2010). Neurog2 controls the leading edge of neurogenesis in the mammalian retina. *Dev. Biol.* 340, 490–503. doi: 10.1016/j.ydbio.2010.02.002
- Jadhav, A. P., Roesch, K., and Cepko, C. L. (2009). Development and neurogenic potential of Muller glial cells in the vertebrate retina. *Prog. Retin. Eye Res.* 28, 249–262. doi: 10.1016/j.preteyeres.2009.05.002
- Jorstad, N. L., Wilken, M. S., Grimes, W. N., Wohl, S. G., Vandenbosch, L. S., Yoshimatsu, T., et al. (2017). Stimulation of functional neuronal regeneration from Muller glia in adult mice. *Nature* 548, 103–107. doi: 10.1038/nature23283
- Karl, M. O., Hayes, S., Nelson, B. R., Tan, K., Buckingham, B., and Reh, T. A. (2008). Stimulation of neural regeneration in the mouse retina. *Proc. Natl. Acad. Sci. U.S.A.* 105, 19508–19513. doi: 10.1073/pnas.0807453105
- Karl, M. O., and Reh, T. A. (2012). Studying the generation of regenerated retinal neuron from Muller glia in the mouse eye. *Methods Mol. Biol.* 884, 213–227. doi: 10.1007/978-1-61779-848-1\_15
- Kimura, A., Namekata, K., Guo, X., Noro, T., Harada, C., and Harada, T. (2017). Targeting oxidative stress for treatment of glaucoma and optic neuritis. *Oxid. Med. Cell Longev.* 2017:2817252. doi: 10.1155/2017/2817252
- Lawrence, J. M., Singhal, S., Bhatia, B., Keegan, D. J., Reh, T. A., Luthert, P. J., et al. (2007). MIO-M1 cells and similar muller glial cell lines derived from adult human retina exhibit neural stem cell characteristics. *Stem Cells* 25, 2033–2043. doi: 10.1634/stemcells.2006-0724
- Lee, J. H., Choy, M. L., and Marks, P. A. (2012). Mechanisms of resistance to histone deacetylase inhibitors. *Adv. Cancer Res.* 116, 39–86. doi: 10.1016/B978-0-12-394387-3.00002-1
- Liang, Y. B., Zhang, Y., Musch, D. C., and Congdon, N. (2017). Proposing new indicators for glaucoma healthcare service. *Eye Vis.* 4:6. doi: 10.1186/s40662-017-0071-0
- Lin, Y. P., Ouchi, Y., Satoh, S., and Watanabe, S. (2009). Sox2 plays a role in the induction of amacrine and Muller glial cells in mouse retinal progenitor cells. *Invest. Ophthalmol. Vis. Sci.* 50, 68–74. doi: 10.1167/iovs.07-1619
- Livak, K. J., and Schmittgen, T. D. (2001). Analysis of relative gene expression data using real-time quantitative PCR and the 2<sup>-</sup>(Delta Delta C(T)) Method. *Methods* 25, 402–408. doi: 10.1006/meth.2001.1262
- Loffler, K., Schafer, P., Volkner, M., Holdt, T., and Karl, M. O. (2015). Age-dependent Muller glia neurogenic competence in the mouse retina. *Glia* 63, 1809–1824. doi: 10.1002/glia.22846
- Macosko, E. Z., Basu, A., Satija, R., Nemes, J., Shekhar, K., Goldman, M., et al. (2015). Highly parallel genome-wide expression profiling of individual cells using nanoliter droplets. *Cell* 161, 1202–1214. doi: 10.1016/j.cell.2015.05.002
- Martersteck, E. M., Hirokawa, K. E., Everts, M., Bernard, A., Duan, X., Li, Y., et al. (2017). Diverse central projection patterns of retinal ganglion cells. *Cell Rep.* 18, 2058–2072. doi: 10.1016/j.celrep.2017.01.075
- Masserdotti, G., Gillotin, S., Sutor, B., Drechsel, D., Irmeler, M., Jorgensen, H. F., et al. (2015). Transcriptional mechanisms of proneural factors and REST in regulating neuronal reprogramming of astrocytes. *Cell Stem Cell* 17, 74–88. doi: 10.1016/j.stem.2015.05.014
- Matsuda, T., and Cepko, C. L. (2004). Electroporation and RNA interference in the rodent retina *in vivo* and *in vitro*. *Proc. Natl. Acad. Sci. U.S.A.* 101, 16–22. doi: 10.1073/pnas.2235688100
- Matsuda, T., and Cepko, C. L. (2007). Controlled expression of transgenes introduced by *in vivo* electroporation. *Proc. Natl. Acad. Sci. U.S.A.* 104, 1027–1032. doi: 10.1073/pnas.0610155104
- Nelson, B. R., Ueki, Y., Reardon, S., Karl, M. O., Georgi, S., Hartman, B. H., et al. (2011). Genome-wide analysis of Muller glial differentiation reveals a requirement for Notch signaling in postmitotic cells to maintain the glial fate. *PLoS ONE* 6:e22817. doi: 10.1371/journal.pone.0022817
- Nickerson, P. E., Da Silva, N., Myers, T., Stevens, K., and Clarke, D. B. (2008). Neural progenitor potential in cultured Muller glia: effects of passaging and exogenous growth factor exposure. *Brain Res.* 1230, 1–12. doi: 10.1016/j.brainres.2008.03.095
- Nickerson, P. E., Mcleod, M. C., Myers, T., and Clarke, D. B. (2011). Effects of epidermal growth factor and erythropoietin on Muller glial activation and phenotypic plasticity in the adult mammalian retina. *J. Neurosci. Res.* 89, 1018–1030. doi: 10.1002/jnr.22629

- Ooto, S., Akagi, T., Kageyama, R., Akita, J., Mandai, M., Honda, Y., et al. (2004). Potential for neural regeneration after neurotoxic injury in the adult mammalian retina. *Proc. Natl. Acad. Sci. U.S.A.* 101, 13654–13659. doi: 10.1073/pnas.0402129101
- Pollak, J., Wilken, M. S., Ueki, Y., Cox, K. E., Sullivan, J. M., Taylor, R. J., et al. (2013). ASCL1 reprograms mouse Muller glia into neurogenic retinal progenitors. *Development* 140, 2619–2631. doi: 10.1242/dev.091355
- Quina, L. A., Pak, W., Lanier, J., Banwait, P., Gratwick, K., Liu, Y., et al. (2005). Brn3a-expressing retinal ganglion cells project specifically to thalamocortical and collicular visual pathways. *J. Neurosci.* 25, 11595–11604. doi: 10.1523/JNEUROSCI.2837-05.2005
- Rapaport, D. H., Wong, L. L., Wood, E. D., Yasumura, D., and Lavail, M. M. (2004). Timing and topography of cell genesis in the rat retina. *J. Comp. Neurol.* 474, 304–324. doi: 10.1002/cne.20134
- Raposo, A. A., Vasconcelos, F. F., Drechsel, D., Marie, C., Johnston, C., Dolle, D., et al. (2015). Ascl1 coordinately regulates gene expression and the chromatin landscape during neurogenesis. *Cell Rep.* 10, 1544–1556. doi: 10.1016/j.celrep.2015.02.025
- Rodriguez, A. R., De Sevilla Muller, L. P., and Brecha, N. C. (2014). The RNA binding protein RBPMS is a selective marker of ganglion cells in the mammalian retina. *J. Comp. Neurol.* 522, 1411–1443. doi: 10.1002/cne.23521
- Rolf, B., Lang, D., Hillenbrand, R., Richter, M., Schachner, M., and Bartsch, U. (2003). Altered expression of CHL1 by glial cells in response to optic nerve injury and intravitreal application of fibroblast growth factor-2. *J. Neurosci. Res.* 71, 835–843. doi: 10.1002/jnr.10533
- Sanes, J. R., and Masland, R. H. (2015). The types of retinal ganglion cells: current status and implications for neuronal classification. *Annu. Rev. Neurosci.* 38, 221–246. doi: 10.1146/annurev-neuro-071714-034120
- Singhal, S., Bhatia, B., Jayaram, H., Becker, S., Jones, M. F., Cottrill, P. B., et al. (2012). Human Muller glia with stem cell characteristics differentiate into retinal ganglion cell (RGC) precursors *in vitro* and partially restore RGC function *in vivo* following transplantation. *Stem Cells Transl. Med.* 1, 188–199. doi: 10.5966/sctm.2011-0005
- Song, M. R., and Ghosh, A. (2004). FGF2-induced chromatin remodeling regulates CNTF-mediated gene expression and astrocyte differentiation. *Nat. Neurosci.* 7, 229–235. doi: 10.1038/nn1192
- Song, W. T., Zhang, X. Y., and Xia, X. B. (2013). Atoh7 promotes the differentiation of retinal stem cells derived from Muller cells into retinal ganglion cells by inhibiting Notch signaling. *Stem Cell Res. Ther.* 4:94. doi: 10.1186/scrt305
- Todd, L., Volkov, L. I., Zelinka, C., Squires, N., and Fischer, A. J. (2015). Heparin-binding EGF-like growth factor (HB-EGF) stimulates the proliferation of Muller glia-derived progenitor cells in avian and murine retinas. *Mol. Cell Neurosci.* 69, 54–64. doi: 10.1016/j.mcn.2015.10.004
- Torper, O., and Gotz, M. (2017). Brain repair from intrinsic cell sources: Turning reactive glia into neurons. *Prog. Brain Res.* 230, 69–97. doi: 10.1016/bs.pbr.2016.12.010
- Turner, D. L., Snyder, E. Y., and Cepko, C. L. (1990). Lineage-independent determination of cell type in the embryonic mouse retina. *Neuron* 4, 833–845. doi: 10.1016/0896-6273(90)90136-4
- Ueki, Y., Wilken, M. S., Cox, K. E., Chipman, L., Jorstad, N., Sternhagen, K., et al. (2015). Transgenic expression of the proneural transcription factor Ascl1 in Muller glia stimulates retinal regeneration in young mice. *Proc. Natl. Acad. Sci. U.S.A.* 112, 13717–13722. doi: 10.1073/pnas.1510595112
- Wilken, M. S., and Reh, T. A. (2016). Retinal regeneration in birds and mice. *Curr. Opin. Genet. Dev.* 40, 57–64. doi: 10.1016/j.gde.2016.05.028
- Wohl, S. G., and Reh, T. A. (2016). miR-124-9-9\* potentiates Ascl1-induced reprogramming of cultured Muller glia. *Glia* 64, 743–762. doi: 10.1002/glia.22958
- Wong-Riley, M. T. (2010). Energy metabolism of the visual system. *Eye Brain* 2, 99–116. doi: 10.2147/EB.S9078
- Wu, Z. K., Cao, L., Zhang, X. Y., Song, W. T., and Xia, X. B. (2016). Promotion on the differentiation of retinal Muller cells into retinal ganglion cells by Brn-3b. *Int. J. Ophthalmol.* 9, 948–954. doi: 10.18240/ijo.2016.07.03
- Yang, W., and Yuste, R. (2017). *In vivo* imaging of neural activity. *Nat. Methods* 14, 349–359. doi: 10.1038/nmeth.4230
- Yao, K., Qiu, S., Wang, Y. V., Park, S. J. H., Mohns, E. J., Mehta, B., et al. (2018). Restoration of vision after *de novo* genesis of rod photoreceptors in mammalian retinas. *Nature* 560, 484–488. doi: 10.1038/s41586-018-0425-3
- Young, R. W. (1985). Cell differentiation in the retina of the mouse. *Anat. Rec.* 212, 199–205. doi: 10.1002/ar.1092120215

**Conflict of Interest Statement:** The authors declare that the research was conducted in the absence of any commercial or financial relationships that could be construed as a potential conflict of interest.

Copyright © 2018 Guimarães, Landeira, Coelho, Golbert, Silveira, Linden, de Melo Reis and Costa. This is an open-access article distributed under the terms of the Creative Commons Attribution License (CC BY). The use, distribution or reproduction in other forums is permitted, provided the original author(s) and the copyright owner(s) are credited and that the original publication in this journal is cited, in accordance with accepted academic practice. No use, distribution or reproduction is permitted which does not comply with these terms.